International Mathematical Forum, Vol. 7, 2012, no. 48, 2373 - 2392

Temperature Distribution in Living Biological Tissue Simultaneously Subjected to Oscillatory Surface and Spatial Heating: Analytical and Numerical Analysis

Emmanuel Kengne[1,2], Ahmed Lakhssassi[1] and Rémi Vaillancourt[2]

[1] Laboratoire d'ingénierie des microsystèmes avancés
Département d'informatique et d'ingénierie
Université du Québec en Outaouais
101 St-Jean-Bosco, Succursale Hull
Gatineau (QC) J8Y 3G5, Canada

[2]Department of Mathematics and Statistics
University of Ottawa, 585 King Edward Ave.
Ottawa, ON K1N 6N5, Canada

Corresponding author: E. Kengne, e-mail: kengem01@uqo.ca

The first author, Emmanuel Kengne dedicates this work to the memory of their beloved son, Fred Jake Sado

Abstract

To predict temperature distribution in a finite biological tissue simultaneously subjected to oscillatory surface and spatial heating, we apply a nonlinear one-dimensional temperature-dependent blood perfusion bioheat Pennes transfer equation. Going from works of Jens Lang et al. in *IEEE Trans. on Biomedical Engineering* (1999) pp. 1129–138 and Tzu-Ching et al. in *Medical Engineering & Physics* 29 (2007) pp. 946–953, we investigate analytically and numerically the effect of various blood and heating parameters on the temperature distribution in muscle, tumor, fat, dermis, and subcutaneous tissues.

PACS: 42.65.Tg, 42.25.Bs, 84.40.Az, 02.60.Cb

Keywords: Temperature-dependent blood perfusion; Bioheat Pennes transfer equation; Steady-state temperature fields; Muscle tissue; Fat tissue; Tumor tissue

1 Introduction

The temperature distribution of skin, mainly used in medicine for diagnosis [13, 18, 15, 24], for follow-up treatments [22], or for the study of the physiological functions of healthy individuals [19], has become a large domain of scientific research and attracts the attention of several researchers. Since Pennes' pioneering work of 1948 [16], almost all investigations on temperature distribution of skin are based on the bioheat transfer equation [17, 6, 2, 5, 9]

$$\rho c \frac{\partial T}{\partial t} = \operatorname{div}(k \operatorname{grad} T) - c_b W (T - T_b) + Q. \tag{1}$$

Here, ρ, c, and k are the density, specific heat, and thermal conductivity of tissue, respectively; c_b and T_b stand for specific heat of the blood and blood temperature (also called arterial temperature), respectively; W is the mass flow rate of blood per unit volume of tissue; Q is the rate of the heat per unit volume of tissue produced by the source; T is local tissue temperature.

Pennes eq. (1) which accounts for the ability of tissue to remove heat by both passive conduction (diffusion) and perfusion of tissue by blood, is generally used to model many of the bioheat transfer problems. The original work of Pennes [16] assumed a constant-rate blood perfusion of the form $W = V\rho_b$, where V and ρ_b are respectively the perfusion rate per unit volume of tissues and the density of the blood. In this case, $V\rho_b c_b (T_b - T)$ models the effect of perfusion and does not include the specific case of temperature dependent perfusion. However, vascularized tissue often experiences increased perfusion as temperature increases [4, 20, 21]. To include the specific case of temperature dependent perfusion, it is then necessary to consider a general form of Eq. (1) in which the blood perfusion rate W is a function of temperature T (see for example Refs. [13, 7, 11, 10, 12]).

In this paper we consider a special case of the one-dimensional (1-D) Pennes bioheat transfer equation with a constant thermal conductivity of tissue:

$$k\frac{\partial^2 T}{\partial x^2} = \rho c\frac{\partial T}{\partial t} + c_b W_b (T - T_b) + c_b \rho_b W_m (T)(T - T_b) + Q_{\text{met}} + Q_{\text{hs}}. \tag{2}$$

Here, x $(0 \le x \le L)$ gives the distance from the skin surface to the body core (in m), t is the time (in s), and $T = T(x,t)$ measures the local temperature at depth x from the surface at time t; L is the distance (in m) between the skin surface and the body core. Therefore, we assume in our investigation that the skin surface is defined at $x = 0$ while the body core at $x = L$. Q_{met} is the metabolic heat generation per volume, and $Q_{\text{hs}} = Q_{\text{hr}}(x,t)$ the heat source due to spatial heating. The 1-D case of Pennes bioheat transfer equation is a good approximation when heat mainly propagates in the direction perpendicular to the skin surface. Comparing Eq. (2) and Eq. (1), it is clear that temperature-dependent blood perfusion reads

$$W = W_b + \rho_b W_m (T). \tag{3}$$

To completely determine the temperature distribution, it is necessary to associate boundary conditions with the the differential equation (2). In our case, we associate with Eq. (2) the oscillatory heat flux boundary condition which is described as follows [18]

$$-k\frac{\partial T}{\partial x}\bigg|_{x=0} = q_0 \exp(i\omega t), \tag{4}$$

where q_0 and ω are the heat flux on the skin surface and the heating frequency, respectively; here, $q_0 \exp(i\omega t)$ is the time-dependent surface heat flux. No heat loss is assumed at $x = L$ and the body core temperature is regarded as constant (T_c) on considering that the biological body tends to keep its core temperature to be stable

$$T(x,t)|_{x=L} = T_c. \tag{5}$$

The aim of the present work is to investigate, under a temperature-dependent blood perfusion, the temperature distribution in biological living tissue simultaneously subjected to oscillatory surface and spatial heating. We restrict ourselves to healthy tissue (muscle and fat), tumor tissue, dermis and subcutaneous tissues. Following J. Lang et al. [13], the present work is carried out under the following conditions:

(a) For blood, $T_b = 37°\text{C}$, $\rho_b = 1060$ kg/m^3, and $c_b = 3500$ Ws/kg/°C;

(b) Mean perfusion values for muscle and fat and maximal value for tumor if a constant-rate perfusion model is applied: $W_{\text{muscle}} = 2.3\text{kg/s/m}^3$, $W_{\text{fat}} = 0.54\text{kg/s/m}^3$, and $W_{\text{tumor}} = 0.833\text{kg/s/m}^3$.

Table 1: Material properties of tissues

Tissue	Thermal conductivity (k[W/m/°C])	Density(ρ [kg/m^3])	Specific heat (c [Ws/kg/°C])
Muscle	0.642	$1,000$	$3,500$
Tumor	0.642	$1,000$	$3,500$
Fat	0.210	900	$3,500$
Dermis	0.450	$1,200$	$3,300$
Subcutaneous	0.190	$1,000$	$2,675$

(c) The temperature-dependent on blood perfusion (3) is taken as follows:

(i) Temperature-dependent of blood perfusion in muscle

$$\mathrm{W}_{\mathrm{muscle}}(T) = \begin{cases} 0.45 + 3.55\exp\left(-(T-45)^2/12\right), & \text{if } T \le 45, \\ 4.0, & \text{if } T > 45; \end{cases} \tag{6}$$

(ii) Temperature-dependent of blood perfusion in fat

$$\mathrm{W}_{\mathrm{fat}}(T) = \begin{cases} 0.36 + 0.36\exp\left(-(T-45)^2/12\right), & \text{if } T \le 45, \\ 0.72, & \text{if } T > 45; \end{cases} \tag{7}$$

(iii) Temperature-dependent of blood perfusion in tumor

$$\mathrm{W}_{\mathrm{tumor}}(T) = \begin{cases} 0.833, & \text{if } T < 37, \\ 0.833(T-37)^{4.8}/5438, & \text{if } 37 \le T \le 42, \\ 0.416, & \text{if } T > 42. \end{cases} \tag{8}$$

(iv) Temperature-dependent of blood perfusion in dermis and subcutaneous

$$\mathrm{W}_{\mathrm{der\ \&\ sub}}(T) = \omega_0(1+\gamma T), \tag{9}$$

where ω_0 and γ are the baseline perfusion and the linear coefficient of temperature dependence, respectively.

(d) The other parameters to be used in the numerical simulation (they have been taken from work [13]).

Throughout this paper, the body core temperature, the heat flux on the skin surface, and the metabolic heat generation are taken as $T_c = 37°\mathrm{C}$, $q_0 = 500\mathrm{W/m}^2$, and $Q_{\mathrm{met}} = 33,800\ \mathrm{W/m}^3$, respectively, (see Refs. [13, 18, 8]). Also, the distance between the skin surface and the body core is taken to be $L = 0.02\mathrm{m}$ (see for example [14, 23, 3] where it is shown that the interior tissue temperature usually tends to a constant within a short distance such as 0.02–0.03 m).

The rest of the paper is organized as follows: Section 2 looks at the analytical solutions of problem (2), (4)–(5) for a constant blood perfusion. In section 3, we consider the temperature-dependent blood perfusion and present numerical solutions of problem (2), (4)–(5). Section 4 concludes and summarizes the results.

2 Analytical solution of problem (2), (4)–(5) for a constant blood perfusion

In this section, we find the solution of problem (2), (4)–(5) when blood perfusion does not depend on temperature, i.e., when $W_m(T) \equiv 0$. A special investigation is carried out when heat flux decays exponentially with the distance from the skin surface.

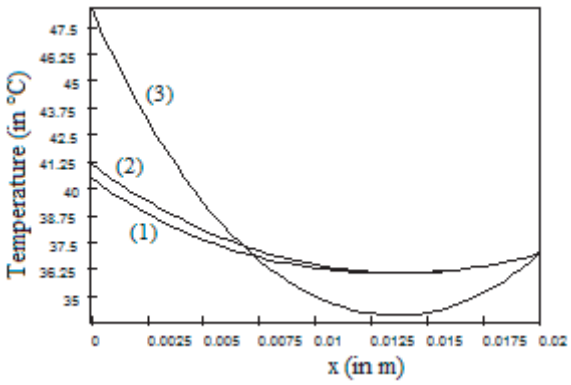

Figure 1: Initial temperature vs x for muscle tissue (1),tumor tissue (2), and fat tissue (3).

2.1 Heat transfer in tissues in the general case of heat flux

In this subsection section, we start by finding the initial condition for problem (2), (4)–(5); in fact, to evaluate the transient tissue temperature field due to varied environment, the steady state temperature distribution which represents the basal state of living tissues needs to be known. We denote by $T_0(x)$ the initial temperature of the skin. In other words, the steady-state temperature fields prior to heating is assumed to be $T(x,0) = T_0(x)$. It is clear that the heat source is absent prior to heating, meaning that $Q_{\text{hs}}(x,t)|_{t=0} = 0$. The problem of finding $T_0(x)$ reads

$$\begin{cases} k\frac{d^2(T_0-T_b)}{dx^2} = c_b W_b (T_0(x) - T_b) + Q_{\text{met}} \\ -k\frac{dT}{dx}\big|_{x=0} = q_0 \\ T_0(x)|_{x=L} = T_c. \end{cases} \tag{10}$$

The solution to Eq. (10) is

$$\begin{aligned} T_0(x) &= T_b - \frac{Q_{\text{met}}}{c_b W_b} + \frac{q_0}{\sqrt{k c_b W_b}} \exp\left(-\sqrt{\frac{c_b W_b}{k}}x\right) \\ &\quad + \frac{1}{\cosh\sqrt{\frac{c_b W_b}{k}}L}\left(T_c - T_b + \frac{Q_{\text{met}}}{c_b W_b} - \frac{q_0}{\sqrt{k c_b W_b}}\exp\left(-\sqrt{\frac{c_b W_b}{k}}L\right)\right)\cosh\sqrt{\frac{c_b W_b}{k}}x. \end{aligned} \tag{11}$$

Figure 1 shows the profile of the initial temperature for muscle tissue (1), fat tissue (3), and tumor tissue (2). Up to a certain critical depth x_{cr} where the minimal initial temperature is reached, the initial temperature for each tissue decreases, and then increases from depth x_{cr} to $L = 0.02$ m, where x_{cr} is 0.0133985 m, 0.01356635 m, and 0.01391942 m for muscle tissue, fat tissue and tumor tissue, respectively. In other words, the tissue temperature first decreases from the skin surface to a given depth x_{cr} and then, is gradually improved.

We now seek the solution of problem (2), (4)–(5) in the form

$$T(x,t) = T_0(x) + (x-L)\frac{q_0}{k}(1 - \exp(i\omega t)) + v(x,t). \tag{12}$$

Transformation (12) then reduces the problem of solving problem (2), (4)–(5) to solving the following

problem

$$k\frac{\partial^2 v}{\partial x^2} = \rho c\frac{\partial v\left(x,t\right)}{\partial t} + c_b W_b v\left(x,t\right) + f\left(x,t\right), \tag{13}$$

$$v\left(x,t\right)|_{t=0} = 0, \tag{14}$$

$$-k\frac{\partial v\left(x,t\right)}{\partial x}\bigg|_{x=0} = 0; \quad v\left(L,t\right)|_{x=L} = 0, \tag{15}$$

where

$$f\left(x,t\right) = c_b W_b\left(x-L\right)\frac{q_0}{k}\left(1-\exp\left(i\omega t\right)\right) - i\rho c\omega\left(x-L\right)\frac{q_0}{k}\exp\left(i\omega t\right) + Q_{\text{hs}}\left(x,t\right). \tag{16}$$

The solution of problem (13)–(15) can be written in the form of a trigonometric series:

$$v\left(x,t\right) = -\frac{2k}{L\rho c}\sum_{n=0}^{+\infty}\left(\exp\left\{-\left(\frac{c_b W_b}{\rho c}+\frac{k}{\rho c}\left[\frac{\pi+2n\pi}{2L}\right]^2\right)t\right\}\int_0^t\int_0^L f\left(\xi,t\right)\cos\frac{\left(\pi+2n\pi\right)\xi}{2L}\,d\xi\,d\tau\right)\cos\frac{\pi+2n\pi}{2L}x. \tag{17}$$

Inserting (17) into (12), we obtain the solution of problem (2), (4)–(5):

$$T\left(x,t\right) = T_0\left(x\right) + \left(x-L\right)\frac{q_0}{k}\left(1-\exp\left(i\omega t\right)\right)$$
$$-\frac{2k}{L\rho c}\sum_{n=0}^{+\infty}\left(\exp\left\{-\left(\frac{c_b W_b}{\rho c}+\frac{k}{\rho c}\left[\frac{\pi+2n\pi}{2L}\right]^2\right)t\right\}\int_0^t\int_0^L f\left(\xi,\tau\right)\cos\frac{\left(\pi+2n\pi\right)\xi}{2L}d\xi d\tau\right)\cos\frac{\pi+2n\pi}{2L}x. \tag{18}$$

It follows from Eq. (18) that the temperature $T\left(x,t\right)$ in the case of constant surface heat flux ($\omega = 0$) satisfies the following two temporal conditions

$$T(x,t)|_{t\to 0} = T_0(x), \tag{19}$$

$$T(x,t)|_{t\to \text{ very large}} = T_0(x), \tag{20}$$

where $T_0\left(x\right)$ is given by Eq. (11). Condition (19) agrees with the initial condition (note that $f\left(x,t\right)$ is a bounded on $[0,\ L]\times[0,\ +\infty)$). Condition (20) shows that for a constant surface heat flux, the initial temperature of the skin coincides with its steady-state temperature. It is important to notice that Eq. (20) is useful to investigate the transient temperature profiles in living tissue when a sinusoidal heating is applied at the skin surface.

2.2 Heat transfer in tissues when heat flux decays exponentially with the distance from the skin surface

In this subsection, we investigate the heat transfer in tissue in the presence of a heat source of the form [3]

$$Q_{\text{hs}}\left(x,t\right) = \eta p\left(t\right)\exp\left(-\eta x\right), \quad x\in[0,\ L],\ t\in[0,\ +\infty), \tag{21}$$

where η is the scattering coefficient and $p\left(t\right)$ the heating power on the skin surface. We first study the case of constant surface heat flux, i.e., when $\omega = 0$, and then, the general case when the surface heat flux depends on time t. Moreover, we will use a spatial sinusoidal heating of the form $Q_{\text{hs}}\left(x,t\right) = \eta\left[p_0 + p_1\cos\omega_p t\right]\exp\left(-\eta x\right)$, meaning that

$$p\left(t\right) = p_0 + p_1\cos\omega_p t. \tag{22}$$

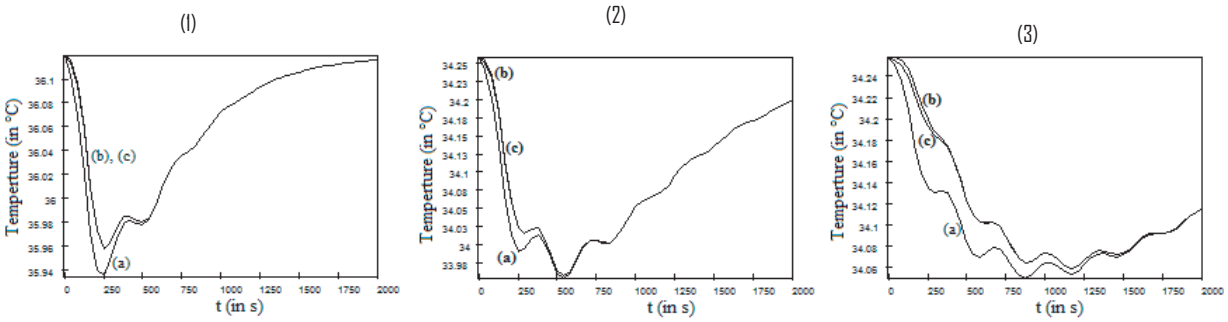

Figure 2: Temperature T vs time t for $x = 0.015$ m, corresponding to muscle tissue (1), tumor tissue (2), and fat tissue (3). (a), (b), and (c) show the first, the second, and the third Fourier series approximation, respectively.

Inserting Eqs. (21) and (22)) into Eq. (17) and coming back to Eq. (18), we find that the temperature in tissue is given by

$$T(x,t) = T_0(x) + (x-L)\frac{q_0}{k}(1-\exp(i\omega t)) - \frac{2k}{L\rho c}\sum_{n=0}^{+\infty} f_n(t)\cos\frac{\pi+2n\pi}{2L}x, \tag{23}$$

where

$$f_n(t) = \frac{2\eta L\left[2L\eta-(-1)^n(1+2n)\pi\exp(-\eta L)\right]}{\pi^2(1+2n)^2+4\eta^2L^2}\left(p_0t-\frac{p_1}{\omega_p}\sin\omega_pt\right)\exp\left\{-\frac{4L^2c_bW_b+k\pi^2(1+2n)^2}{4\rho cL^2}t\right\} \tag{24}$$

if $\omega = 0$, and

$$\begin{aligned} f_n(t) \;=\; & \exp\left\{-\frac{4L^2c_bW_b+k\pi^2(1+2n)^2}{4\rho cL^2}t\right\}\left[\frac{2\eta L\left[2L\eta-(-1)^n(1+2n)\pi\exp(-\eta L)\right]}{\pi^2(1+2n)^2+4\eta^2L^2}\left(p_0t-\frac{p_1}{\omega_p}\sin\omega_pt\right)\right. \\ & \left.-\left(\frac{2L}{\pi+2n\pi}\right)^2\left[c_bW_b\frac{q_0}{k}\left(t+i\frac{\exp(i\omega t)}{\omega}\right)-\rho c\frac{q_0}{k}\exp(i\omega t)+q_0\left(\frac{\omega\rho c-ic_bW_b}{\omega k}\right)\right]\right] \end{aligned} \tag{25}$$

if $\omega \neq 0$.

2.3 Results and discussions

For numerical simulation, we mainly use in Eqs. (24) and (25) with $\eta = 200/\text{m}$, $\omega_p = 0.02$, and $p(t) = 250 + 200\cos\omega_p t$ W/m^2 (see for example Ref. [3])

2.3.1 Effect of constant surface heat flux ($\omega = 0$)

In figure 2, we have plotted the first three Fourier series approximations for temperature T at depth $x = 0.015$ m as function of time t. Lines (a), (b), and (c) correspond to the first, second, and third Fourier series approximation. The plots (1), (2), and (3) give the temperature profile versus t for muscle tissue, tumor tissue, and fat tissue, respectively. These three plots show that for each of the tissues, the temperature is well approximated by any N^{th} Fourier series with $N \geq 2$. For different values of depth x we plotted in figure 3 the third Fourier series approximation, given an approximated temperature in the muscle tissue (1), tumor tissue (2) and fat tissue (3). These plots show that up to a given depth,

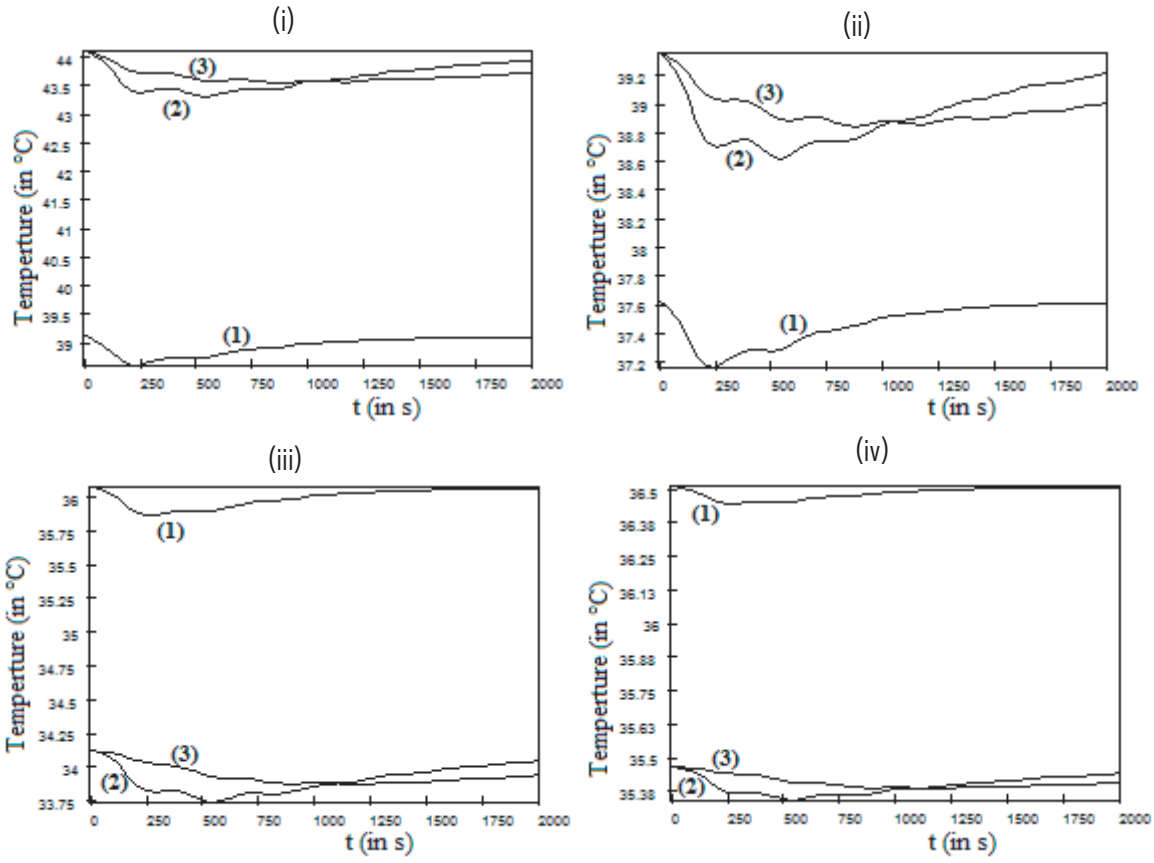

Figure 3: Temperature profile vs time t of different tissues at different depth x. Plots (i), (ii), (iii), and (iv) show the time evolution of temperature at depth $x = 0.02$ m, $x = 0.005$ m, $x = 0.01362809$ m, and $x = 0.018$ m, respectively. Lines (1), (3) and (2) correspond to muscle tissue, fat tissue, and tumor tissue, respectively.

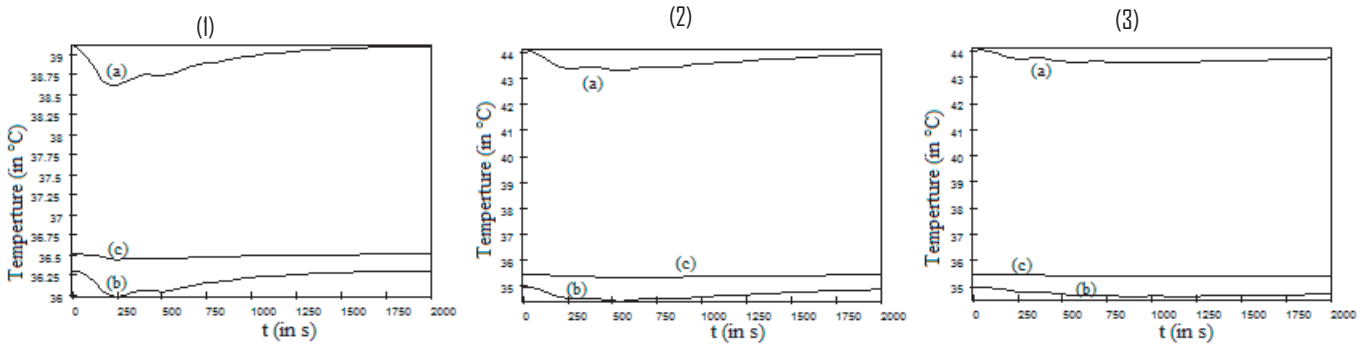

Figure 4: Temperature profile vs time t at different depth x of muscle tissue (1), tumor tissue (2) and fat tissue (2). Plots (a), (b), and (c) show time evolution of temperature at depth $x = 0.02$ m, $x = 0.01$ m, and $x = 0.018$ m, respectively.

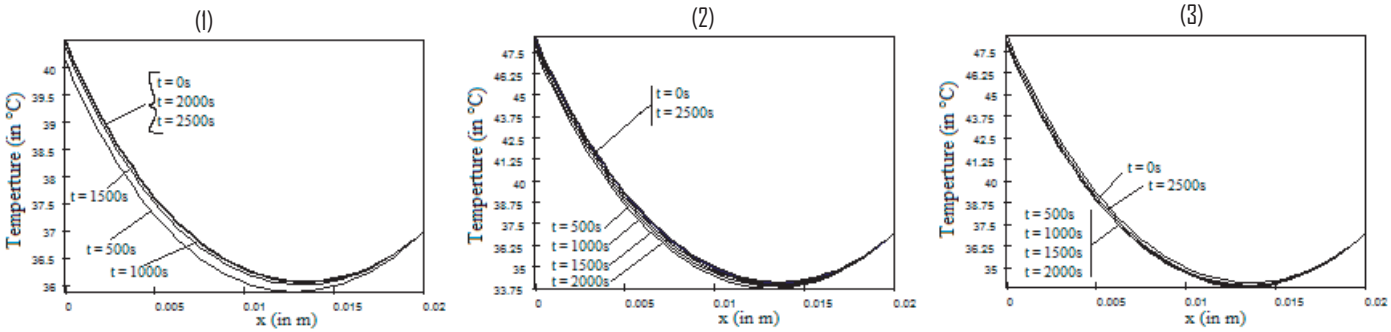

Figure 5: Temperature distribution at different times in muscle tissue (1), tumor tissue (2) and fat tissue (3).

the temperature in muscle tissue is always less than those in fat and tumor tissues, and after this depth, the temperature in muscle tissue becomes superior to those in fat and tumor tissues. If we denote by $\Delta T = T_{\max} - T_{\min}$ the difference between the maximal and the minimal temperatures for all $x \in [0,\ 0.02]$ for the time interval $[0,\ \ t_0]$, then we can conclude from plots 3 that $\min\{\Delta T_{\text{muscle}},\ \Delta T_{\text{fat}},\ \Delta T_{\text{tumor}}\} = \Delta T_{\text{muscle}}$, meaning that the variation of the temperature in muscle tissue is not as great as in fat and tumor tissues. This fact is also confirmed by the plots in figure 4. Here the lines (a), (b), and (c) show the temperature at depth $x = 0.02$ m, $x = 0.01$ m, and $x = 0.018$ m. Plots (1), (2), and (3) refer to the muscle tissue, tumor tissue, and fat tissue, respectively. These two plots also show that the maximal temperature at any depth x of each of the three tissues is reached at the initial time $t = 0$. They also confirm the right boundary condition, that is, for each of the three tissues, the temperature tends to 37°C as $L \to 0.02$ m.

In figure 5, we depict the temperature distributions of muscle tissue (1), tumor tissue (2) and fat tissue (3) at different times. The plots in this figure show that for each tissue and at any time, the tissue temperature first decreases from the skin surface down to some critical depth, and then increases up to the body core. From these plots we conclude that the tissue temperature approaches the initial temperature for large enough time t. In conclusion, the initial temperature also plays the role of steady state temperature in the tissue. A comparison of plots of figures (1), (2), and (3) shows that the tissue temperature in fat tissue slowly approaches the steady state temperature. In fact, the steady state temperature is reached at $t = 2500$ s for muscle and tumor tissues, while it is reached at $t = 5500$ s for fat tissue.

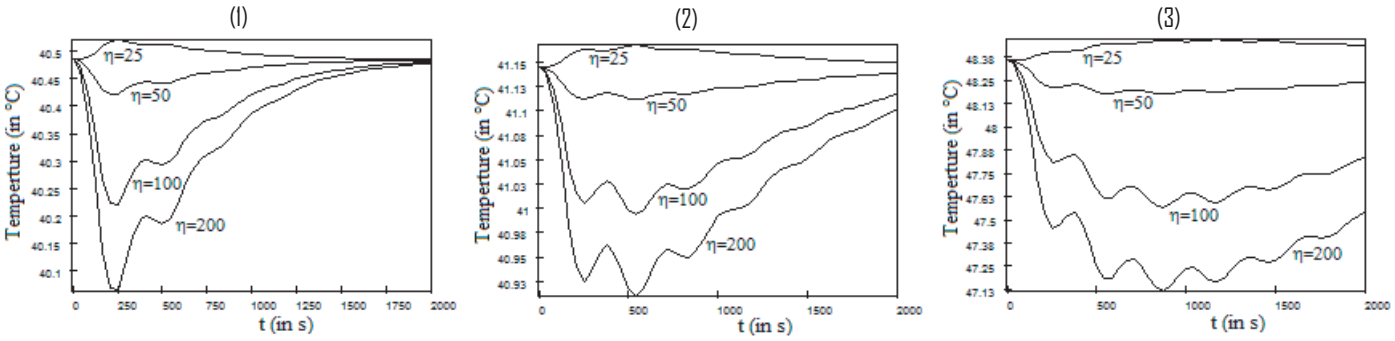

Figure 6: Effect of scattering coefficient on temperature response at skin surface ($x = 0$); plots (1), (2), and (3) refer to muscle tissue, tumor tissue, and fat tissue, respectively

It is evident that the tissue temperature depends not only on time t and depth x, but may also depend on other parameters as for example, on scattering coefficient. Figure 6 shows the effect of scattering coefficient on temperature response at skin surface ($x = 0$). This figure shows that the temperature response at skin surface increases when the scattering coefficient decreases.

2.3.2 Effect of sinusoidal heat flux

Figures 7, 8, and 9 show the effect of sinusoidal heat flux on temperature distribution in the tissue. On figure 7, the first row gives temperature response at skin surface for at different heating frequencies, $\omega = 0.001$, $\omega = 0.005$, and $\omega = 0.01$, while the second one shows the temperature distribution at time $t = 3600$ s for in the absence and in the presence of sinusoidal heat flux. This figure shows how much the sinusoidal heat flux affects the temperature amplitude over the time. From the plots of this figure, we conclude that the presence of sinusoidal heat flux diminishes the temperature amplitude along the tissue depth. Figure 8 gives the temperature profile at a given time along the tissues, when the frequency of sinusoidal heat flux on the skin surface continuously varies from +0 to 0.01. Figure 9, as well as figure 8 shows how the temperature at a given depth from skin surface varies when the heating frequency changes. It is seen from the plots of these last two figures that for a best choice of heating frequency, temperature-fluctuation in the tissue will not be very large at given times (see figure 10).

The plots of figures 10 show the temperature profile along the depth from the skin surface at different heating frequencies and at time $t = 3600$ s. The two horizontal lines in these plots show either the upper bound or the lower bound of the temperature amplitude for a given heating frequency. The difference between the maximal and minimal temperatures for $\omega = 0.006$ is $\Delta T = 24.93°$C for muscle tissue, $\Delta T = 24.33°$C for tumor tissue, and $\Delta T = 40.22°$C for fat tissue. For $\omega = 0.005$, we found that $\Delta T = 2.94°$C for muscle tissue, $\Delta T = 3.42°$C for tumor tissue, and $\Delta T = 17.07°$C for fat tissue, respectively. These calculations show the effect of the heating frequency on the temperature-fluctuation in the skin. It should be noted that the best temperature-fluctuation does not necessary correspond to a smaller heating frequency (see Figs. 8 and 9).

In order to show the effect of the scattering coefficient η on the temperature response in the tissue, we plot in figure 11 the change in temperatures (ΔT) along the tissue depth for different scattering coefficients. More precisely, we took four values of the scattering coefficient, $\eta = 25$/m, $\eta = 50$/m, $\eta = 100$/m, and $\eta = 200$/m and then, plotted in figure 11 $\Delta T = T|_{\eta=25} - T|_{\eta=50}$, $\Delta T = T|_{\eta=50} - T|_{\eta=100}$, and $\Delta T = T|_{\eta=100} - T|_{\eta=200}$. The positivity of all ΔT proves that a smaller scattering coefficient yields a larger temperature in the tissue.

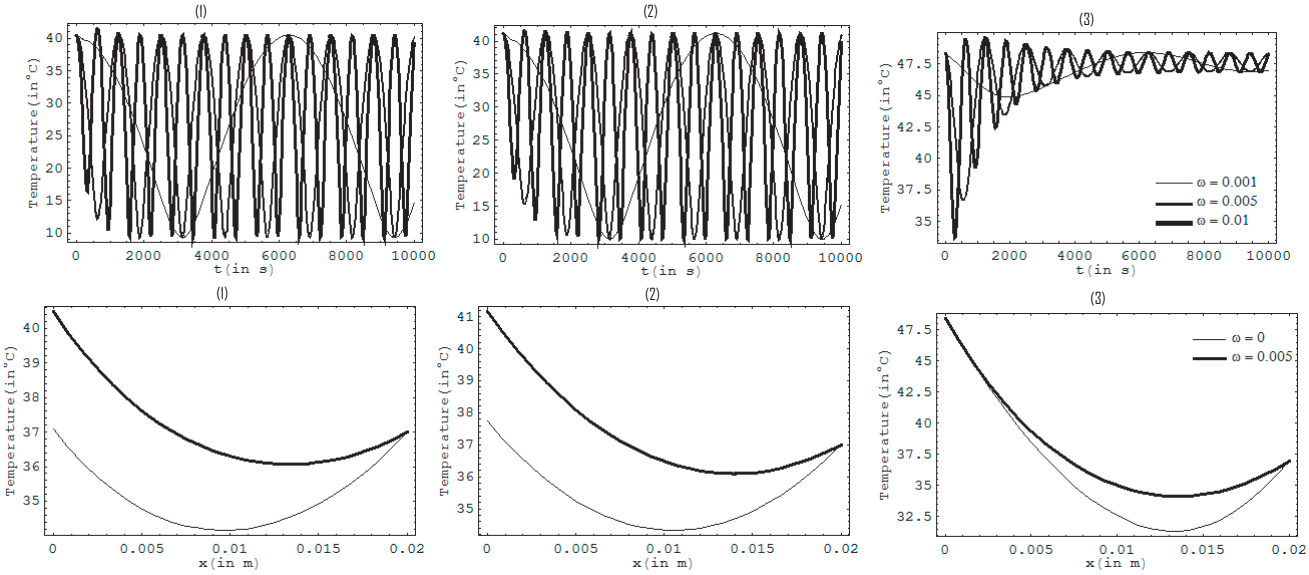

Figure 7: Effect of heating frequency on temperature amplitude at skin surface of muscle tissue (1), tumor tissue (2) and fat tissue (3). The first row shows the temperature response at skin surface, while the second one shows the temperature distribution along the tissue depth at a given time

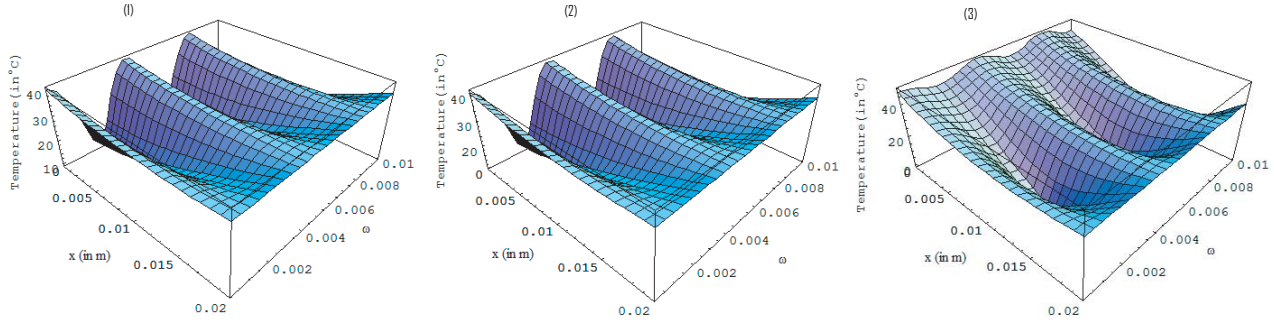

Figure 8: (Color online) Temperature distribution along the tissue depending on the heating frequency, (1), (2), and (3) referring to muscle, tumor and fat tissue, respectively.

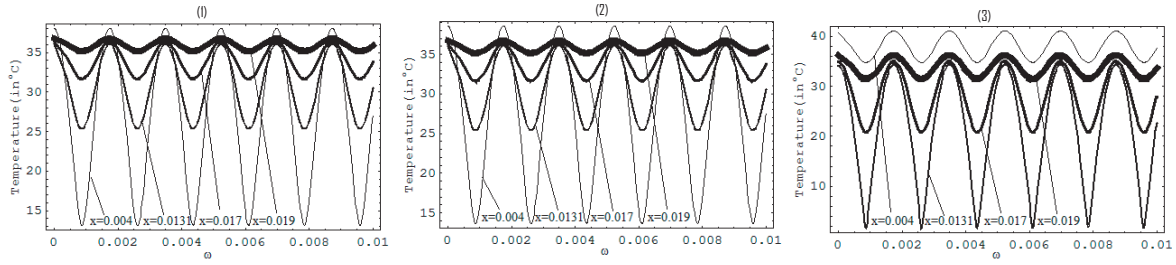

Figure 9: Dependency of the temperature distribution on the heating frequency, (1), (2), and (3) referring to muscle, tumor and fat tissue, respectively.

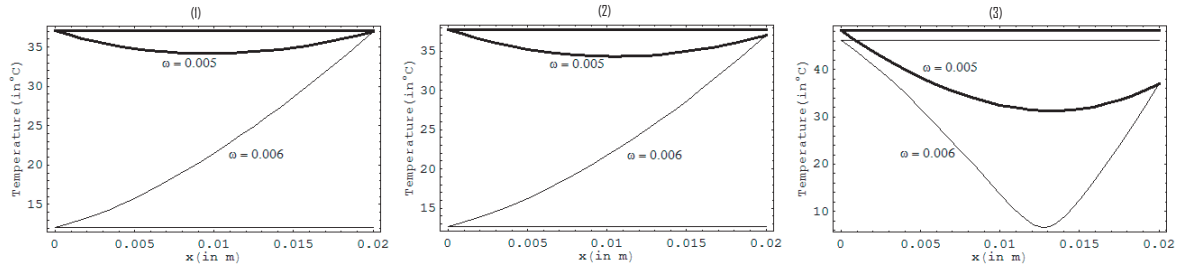

Figure 10: Temperature profile along the tissue depth at different heating frequencies on the skin surface; (1), (2), and (3) refer to muscle, tumor and fat tissue, respectively.

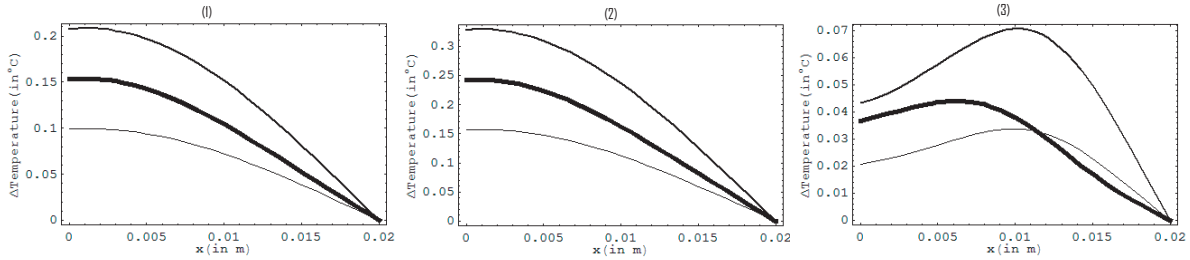

Figure 11: Change in temperatures (ΔT) along the tissue depth for different scattering coefficients, (1), (2), and (3) referring to muscle, tumor and fat tissue, respectively.

3 Solution of problem (2), (4)–(5) for a temperature-dependent blood perfusion

The main difficulties, and even the impossibility of finding an analytical solution of problem (2), (4)–(5), is principally due to the nonlinearity caused by temperature-dependent perfusion. In such a situation, we can limit ourselves to finding numerical solutions of this problem. To find the numerical solution of our problem, in this work we use a two-level finite difference scheme. We use h to represent the space mesh so that L/h will be a positive integer that we denote by N such that $Nh = L$. The time step discretization will be denoted by τ. To construct numerical solutions to problem (2), (4)–(5), we use the second-order central difference scheme in space and the Crank–Nicholson type of scheme in time. In our numerical simulations, we assume that blood perfusion starts to vary with temperature only when a heat source is applied on skin surface. We will choose the initial temperature such that for our model the the maximal temperature in the tissue does not exceed certain temperature limit. Generally, this limit temperature is tissue dependent; for example, it is $T_{\lim} = 44°\mathrm{C}$ for healthy tissues. Our choice of initial temperature is based on the initial temperature in the tissue in the case of constant blood perfusion. In fact, here, we take the initial temperature as the mean value of initial temperature $T_0(x)$ given by Eq. (11). Hence we associate to problem (2), (4)–(5) the initial condition

$$T(x,t)|_{t=0} = \widehat{T}_0(x) = \underset{[0,\ L]}{\mathrm{Mean}}\ T_0(x) \tag{26}$$

(in the case of muscle tissue, fat tissue, and tumor tissue). Let us denote by T_j^{n+1} the numerical temperature at depth x_j at time t_n. The numerical solution to problem (2), (4)–(5) (without the term $c_b W_b (T - T_b)$) with initial condition (26) in vector form reads $\left(T_0^n,\ \overrightarrow{\mathbf{T}}^n\right)^t$, where $\overrightarrow{\mathbf{T}}^n = (T_1^n, ..., T_N^n)^t$.

Using the boundary condition (4), we can express T_0^n in terms of T_1^n :

$$T_0^n = T_1^n + \frac{hq_0}{k}\exp\left(i\omega t_n\right). \tag{27}$$

$\overrightarrow{\mathbf{T}}^n$ is then the solution to the algebraic system

$$\mathbf{Q}_{\text{left}}\,\overrightarrow{\mathbf{T}}^n = \mathbf{Q}_{\text{right}}\,\overrightarrow{\mathbf{T}}^{n-1} + \overrightarrow{\mathbf{F}}, \tag{28}$$

where $\overrightarrow{\mathbf{F}}$ is an $N \times 1$ matrix for which the first and last elements are

$$\frac{\tau q_0}{2h\rho c}\left(\exp\left(i\omega t_{n-1}\right) + \exp\left(i\omega t_n\right)\right) + \frac{\tau}{\rho c}\left(c_b\rho_b W_m\left(T_1^{n-1}\right)T_b - Q_{\text{hs}}\left(x_1, t_{n-1}\right) + c_b W_b T_b - Q_{\text{met}}\right)$$

and T_c, respectively, and each element of the i^{th} row is

$$\frac{\tau}{\rho c}\left(c_b\rho_b W_m\left(T_i^{n-1}\right)T_b - Q_{\text{hs}}\left(x_i, t_{n-1}\right) + c_b W_b T_b - Q_{\text{met}}\right);$$

$\mathbf{Q}_{\text{left}} = (a_{il})$ and $\mathbf{Q}_{\text{right}} = (b_{il})$ are two $N \times N$ square tridiagonal matrices with

$$\begin{aligned}
a_{11} &= 1 + \frac{\tau k}{2h^2\rho c} + \frac{\tau}{2\rho c}\left[c_b W_b + c_b\rho_b W_m\left(T_1^{n-1}\right)\right];\ a_{NN} = 1;\\
a_{ii-1} &= \ a_{ii+1} = -\frac{\tau k}{2h^2\rho c};\\
a_{ii} &= 1 + \frac{\tau k}{h^2\rho c} + \frac{\tau}{2\rho c}\left[c_b W_b + c_b\rho_b W_m\left(T_i^{n-1}\right)\right];\\
b_{11} &= 1 - \frac{\tau k}{2h^2\rho c} - \frac{\tau}{2\rho c}\left[c_b W_b + c_b\rho_b W_m\left(T_1^{n-1}\right)\right];\ b_{NN} = 0;\\
b_{ii-1} &= b_{ii+1} = \frac{\tau k}{2h^2\rho c};\\
b_{ii} &= 1 - \frac{\tau k}{h^2\rho c} - \frac{\tau}{2\rho c}\left[c_b W_b + c_b\rho_b W_m\left(T_i^{n-1}\right)\right].
\end{aligned} \tag{29}$$

It is seen from eqs. (29) that the solution of system (28) exists and is unique. In fact, as we can see from eqs. (29), $\mathbf{Q}_{\text{left}}$ is diagonally dominant. According to Gershgorin theorem [1], $\mathbf{Q}_{\text{left}}$ is invertible.

3.1 Results and discussion

For numerical simulations, we mainly use the following parameters:

$$L = 0.02\text{m},\ T_b = T_c = 37°\text{C},\ \rho_b = 1060\text{kg/m}^3,\ c_b = 3500\text{Ws/kg/°C},\ q_0 = 500\text{W/m}^2,$$
$$Q_{\text{met}} = 33,800\text{W/m}^3,\ \eta = 200/\text{m},\ \omega_p = 0.02,\ \ p_0 = 250,\ p_1 = 200,\ \omega = 0.001,\ \omega_0 = 10\text{ml/100g min}.$$

When talking about the effect of arterial blood temperature T_b, we will use the following values

$$\begin{cases}
T_b = 37°\text{C for a normal human body temperature,}\\
T_b = 34°\text{C in a hypothermia case,}\\
T_b = 39°\text{C in a hyperthermia and fever cases,}\\
T_b = 41°\text{C in a hyperpyrexia case.}
\end{cases} \tag{30}$$

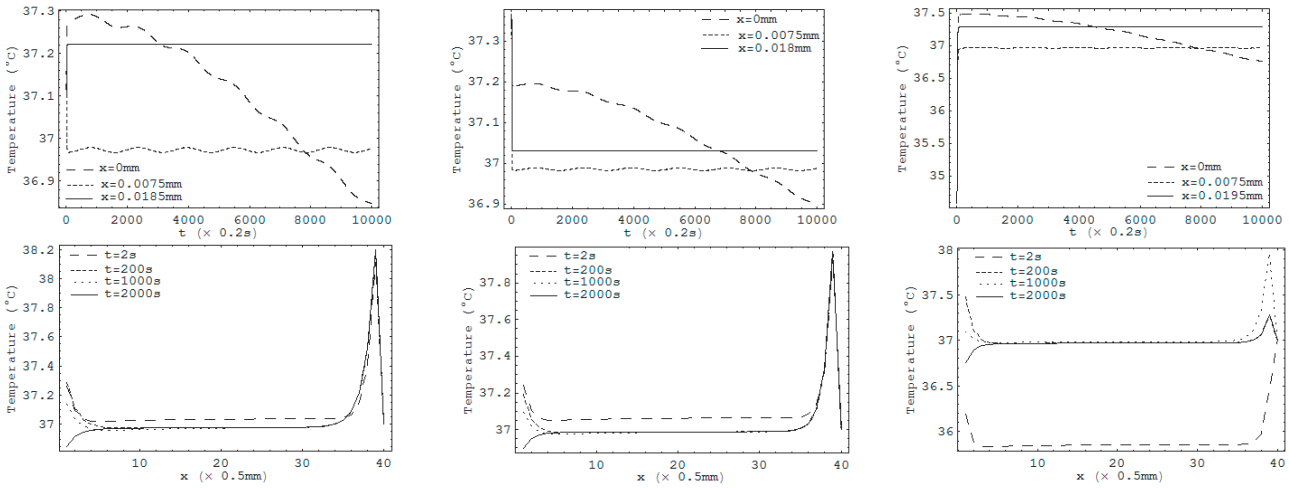

Figure 12: Temporal (top) and spatial (bottom) temperature distribution in biological tissues subject to an oscillatory heat flux with frequency $\omega = 0.001$. Left: Muscle tissue, Middle: Tumor tissue, Right: Fat tissue.

3.1.1 Case of muscle, tumor, and fat tissue

Figures 12 and 13 depict temporal (top) and spatial (bottom) temperature distributions of biological bodies (muscle tissue (left), tumor tissue (middle), and fat tissue (right)) subject to a constant (Fig. 12, with $\omega = 0.001$) and oscillatory (Fig. 13, with $\omega = 0$) heat flux. From the plots showing spatial temperature distribution, we conclude that for muscle tissue and tumor tissue, the temperature decreases with time up to a certain depth, and then increases with time when one approaches the skin core. For fat tissue, the temperature in the tissue increases with time. These plots also show intercross for temperature curves at different times, which indicates the oscillatory aspect of temperature inside the tissue in the presence of both constant and oscillatory heat flux; this situation is confirmed by temporal temperature distribution (top plots). Temperature oscillation inside the tissue in the presence of a constant heat flux is due to the sinusoidal spatial heating (see Eqs. (21) and (22) giving the form of heat source). In the presence of a constant heat flux, skin surface maintains a higher temperature in comparison with temperature inside the tissue. When an oscillatory heat flux is applied on the skin surface, the temperature of the skin surface decreases with time and after a long time of heating reaches an oscillatory steady state below those of all other points: Hence, the oscillatory heat flux leads to a cooling of the surface of the skin. For these three figures, we used $T_b = 37°\text{C}$.

Figures 14, 15, and 16 give out the effect of surface heating frequency ω and the effect of spatial heating frequency ω_p on temperature transients at skin surface. Figure 14 shows temperature profile for different surface heat frequencies when the spatial heating frequency is fixed $\omega_p = 0.02$. On figure 15, we plot temperature curves for different spatial heating frequencies with a fixed surface heating frequency $\omega = 0.001$. Figure 16 shows two scenarios: The first scenario gives out temperature distribution at skin surface when an oscillatory surface heating is applied and a non-oscillatory spatial heating is used; here, $\omega = 0.01$ and $\omega_p = 0$. The second scenario shows temperature distribution at skin surface when the tissue is simultaneously subjected to a constant surface heating ($\omega = 0$) and an oscillatory spatial heating with frequency $\omega_p = 0.01$. We can conclude from the temperature curves of figure 14 that for large values of surface heating frequency, the oscillating effect of spatial heating does not appear. Therefore, an increase of surface heating frequency contributes to a destruction of oscillatory effect of spatial heating (looks like $\omega_p = 0$). Comparing temperature curves of Fig. 14 with those of Fig. 15, it is seen that the variation of surface heating frequency more affects the temperature of surface skin. Our simulations show that temperature mean value at skin surface increases with the spatial heating frequency as well as with surface

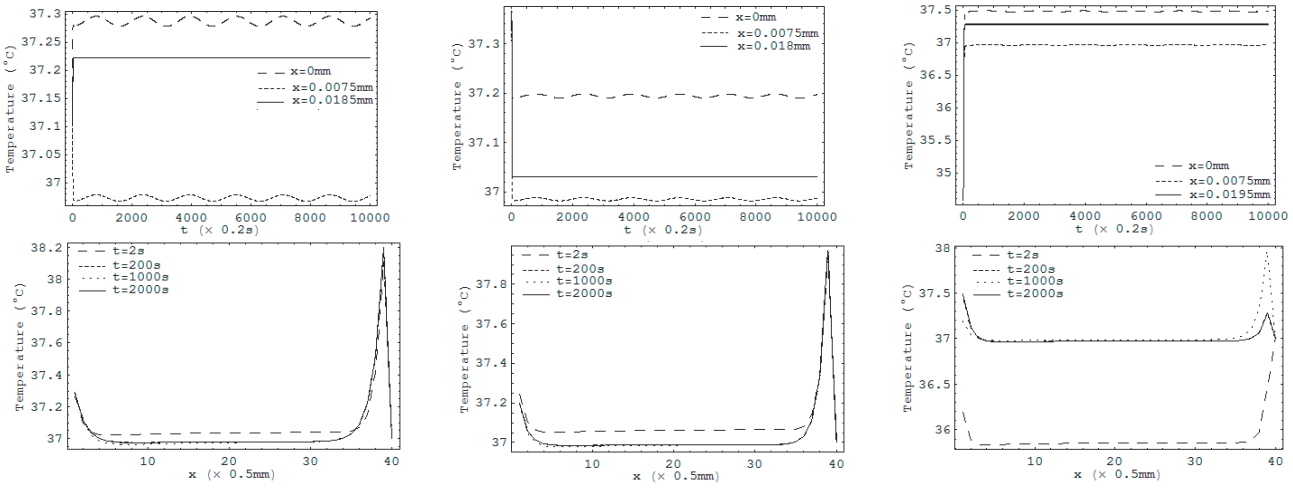

Figure 13: Temporal (top) and spatial (bottom) temperature distribution in biological tissues subject to a constant heat flux (i.e., $\omega = 0$). Left: Muscle tissue, Middle: Tumor tissue, Right: Fat tissue.

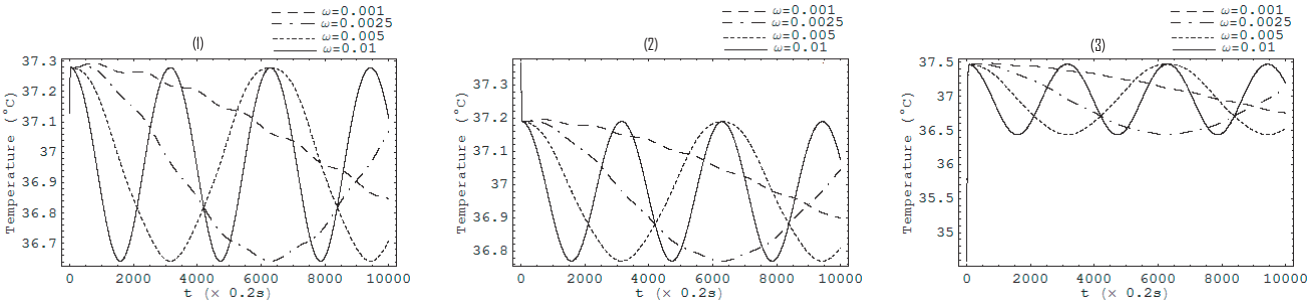

Figure 14: Effect of the surface heating frequency on temperature response at skin surface: (1) muscle tissue; (2) tumor tissue; (3) fat tissue.

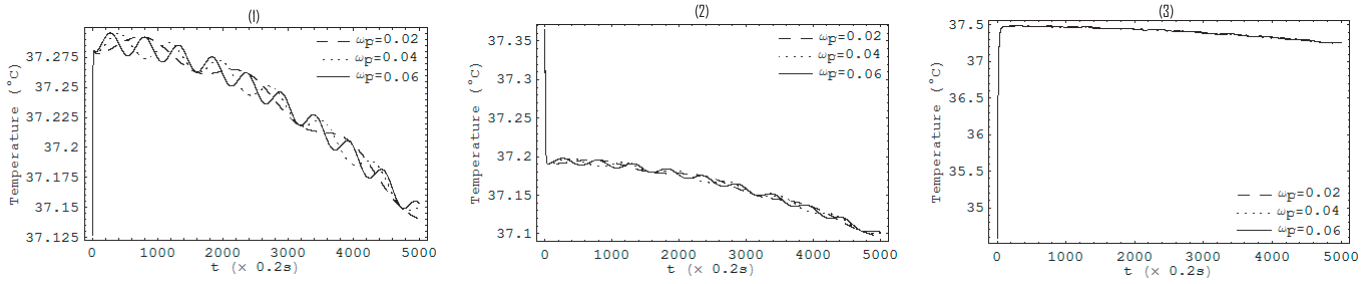

Figure 15: Effect of the spatial heating frequency on temperature response at skin surface: (1) muscle tissue; (2) tumor tissue; (3) fat tissue.

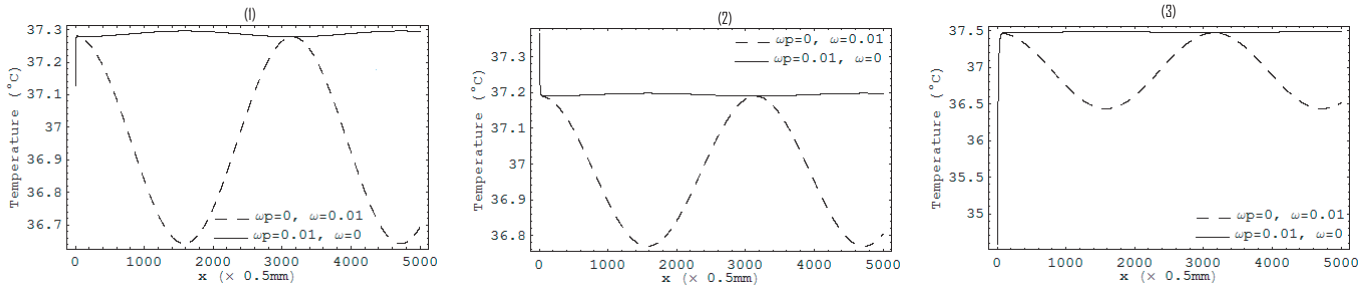

Figure 16: Skin surface temperature response either under oscillatory surface or oscillatory spatial heating: (1) muscle tissue; (2) tumor tissue; (3) fat tissue.

heating frequency (see Figs. 14 and 15). Figure 16 shows that the temperature at skin surface is larger in the case when the tissue is subjected to an oscillatory surface heating ($\omega = 0.01$) and a non-oscillatory spatial heating ($\omega_p = 0$) than in the case when a constant surface heating ($\omega = 0$) and an oscillatory spatial heating ($\omega_p = 0.01$) are applied. Hence, in order to low the temperature at skin surface, it is necessary to apply on skin surface an oscillatory surface heating ($\omega \neq 0$) and a time-independent spatial heating ($\omega_p = 0$). It is clear, as one can see from Figs. 14, 15 and 16 that the frequency of the temperature response varies with that of the surface heating.

Figure 17 depicts the surface temperature transient when tissues were simultaneously subjected to oscillatory surface and spatial heating having the same frequency. The curves of this figure show that when surface and spatial heating have the same frequency, the resulted temperature response

Figure 18 gives out the effect of arterial blood temperature on the temperature transients at skin surface; in this figure, (1), (2), and (3) refer to muscle tissue, tumor tissue, and fat tissue, respectively. The horizontal dash line on the plots of the second row shows the temperature mean value at skin surface. The first row of this figure shows that the larger arterial blood perfusion, the higher temperature increases. As we can see from the curves of the second row, arterial blood temperature does not affect the oscillatory aspect of the temperature at skin surface. We also conclude from figure 18 that the temperature mean value at skin surface is near the arterial blood temperature.

3.1.2 Case of dermis and subcutaneous tissue

For dermis and subcutaneous tissue, we have studied only the case of normal human body temperature; thus we have used 37°C as arterial blood temperature. We worked under the condition that the surface of the tissue was elevated to 37°C at $t = 0$ s.

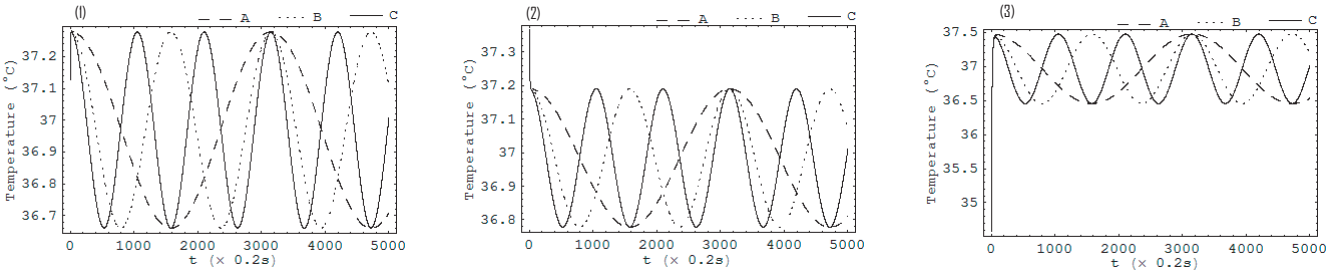

Figure 17: Skin surface temperature response simultaneously under surface and spatial heating with the same frequency; A: $\omega = \omega_p = 0.01$; B: $\omega = \omega_p = 0.02$; C: $\omega = \omega_p = 0.03$. (1): muscle tissue; Column (2): tumor tissue; Column (3): fat tissue.

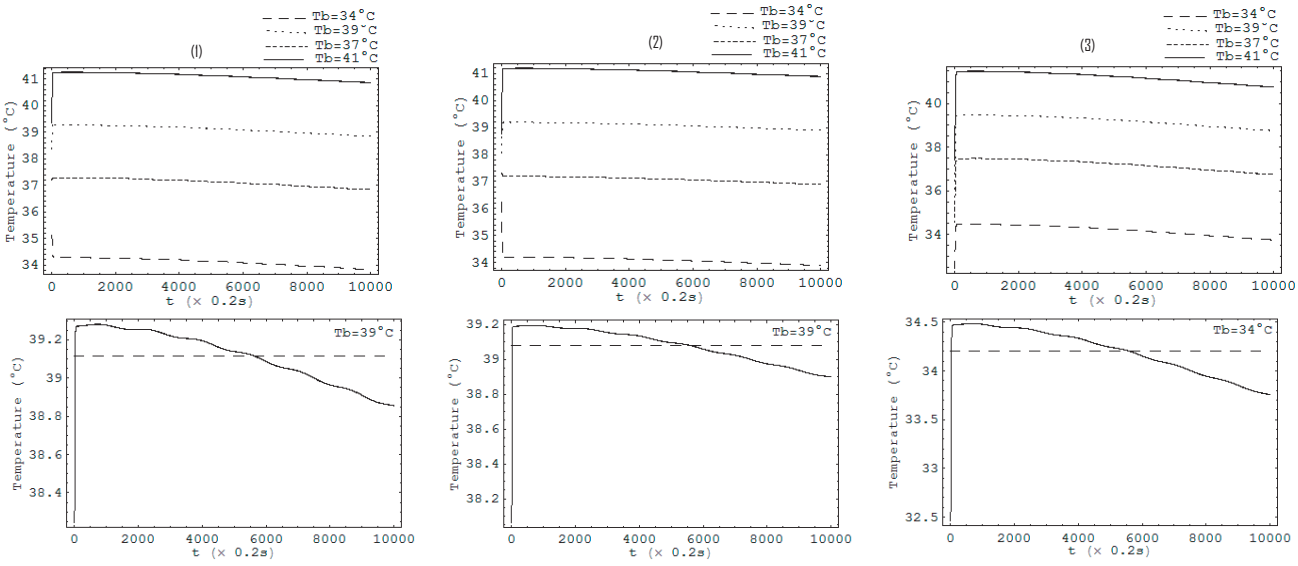

Figure 18: Effect of arterial blood temperature on temperature response at skin surface: Column (1): muscle tissue; Column (2): tumor tissue; Column (3): fat tissue.

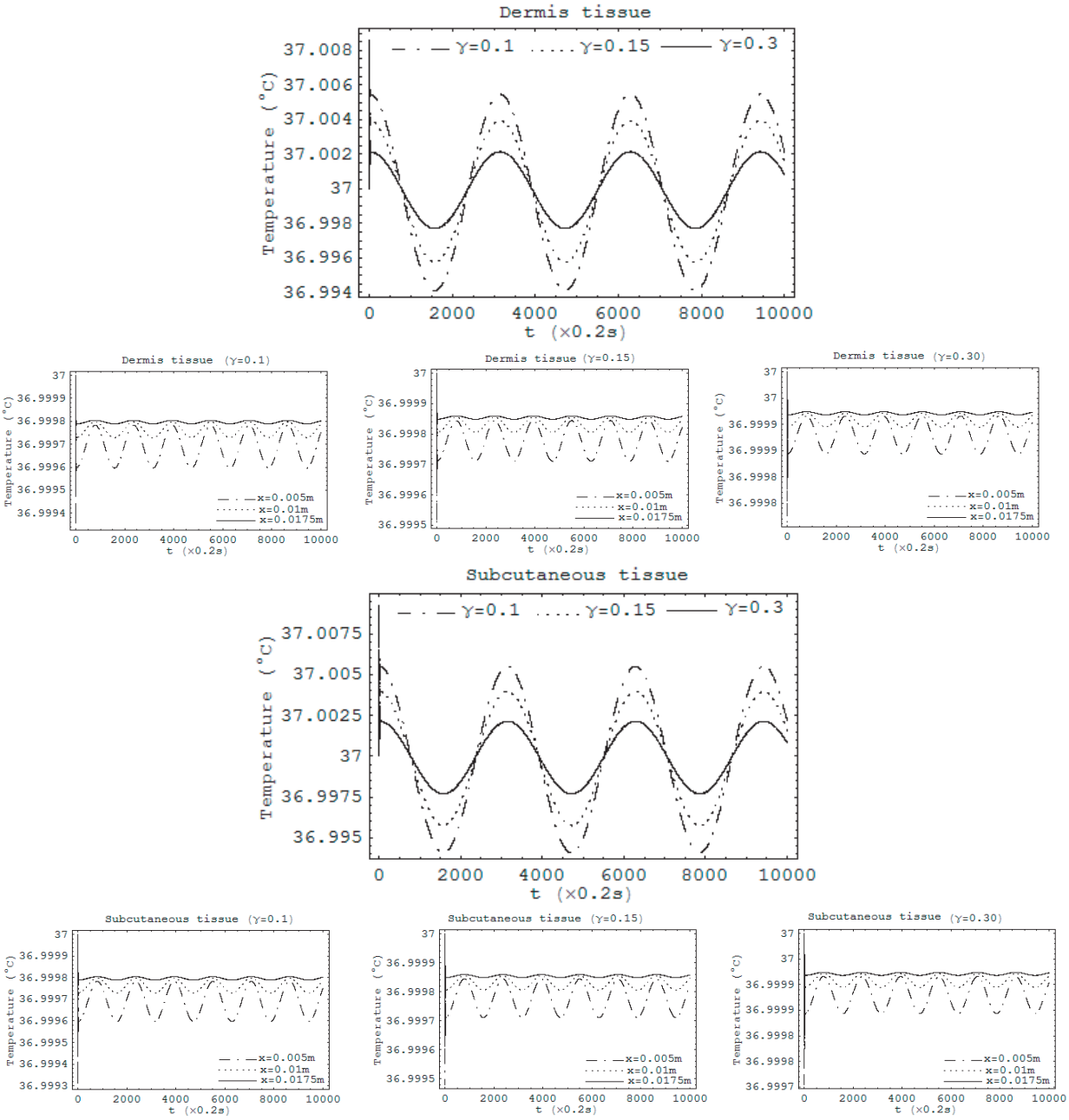

Figure 19: Temporal temperature distribution in dermis and subcutaneous tissue subjected to oscillatory surface and spatial heating. First and third row: Effect of temperature-dependent perfusion at skin surface. Second and fourth row: Temperature distribution at different depths for different blood perfusion. The blood perfusion level was taken to be $\omega_0 = 10\text{ml}/100\text{g min}$.

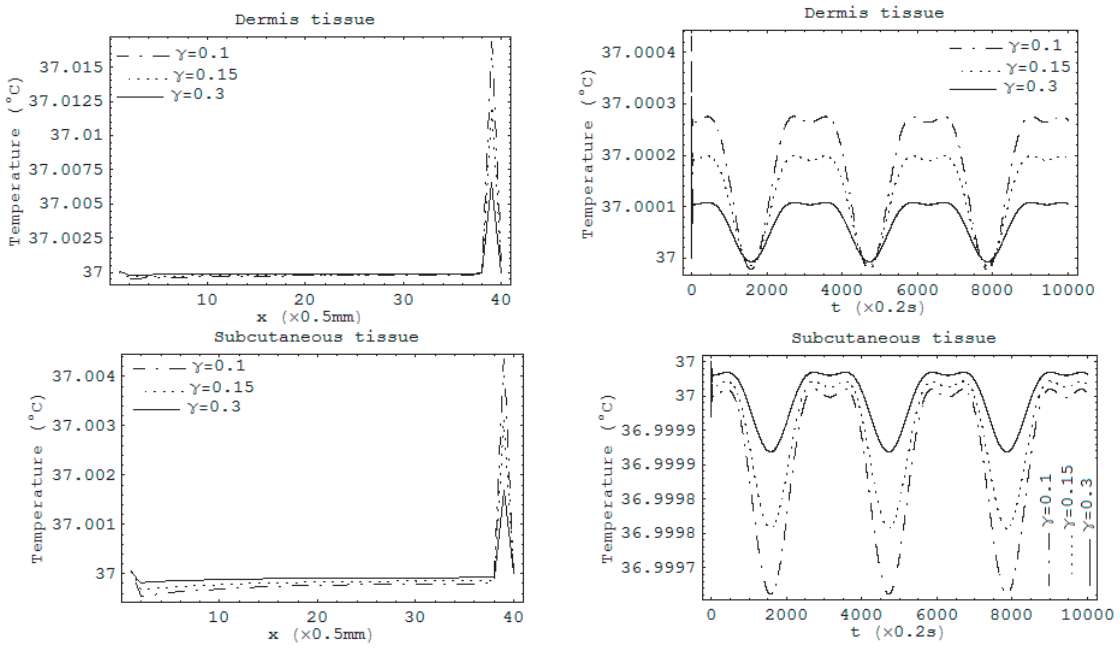

Figure 20: Temperature mean value of dermis and subcutaneous tissue simultaneously subjected to oscillatory surface and spatial heating. Left: Temperature mean value at different depth after 2000s of heating. Right: Temperature mean value of the whole tissue at different time of heating.

Figure 19 depicts temporal temperature distribution for dermis and subcutaneous tissue for different temperature-dependent blood perfusion when the surface of each of the tissues was elevated to 37°C at $t = 0$ s. Temperature curves of the first and third row, as well as those of second and fourth row show that increased perfusion causes a decline in temperature at skin surface. The third and fourth row of Fig. 19 show that decreased blood perfusion causes a decline in temperature inside dermis and subcutaneous tissue. Also from these second and fourth rows it is seen that tissue temperature increases with depth. If instead of varying the linear coefficient γ of the temperature dependence we varied the baseline perfusion ω_0 the same results would be obtained.

Figure 20 gives out the temperature mean value of biological tissue for different values of the linear coefficient γ of temperature dependence. The left curves show the temperature mean value at each depth of dermis and subcutaneous tissue after 2000 s of heating. The right plots show the temperature mean value of the whole biological tissue after a giving time of heating. Here, the surface of the tissue was elevated to 37°C at $t = 0$ s and the baseline perfusion 10ml/100g min has been used. Figure 20 shows that increased blood perfusion causes a rise in the temperature mean value at any depth of dermis and subcutaneous tissue (left plots). Right plots show that at any time of heating, the temperature mean value for dermis tissue is above the temperature of the skin surface at time $t = 0$ s, while that of subcutaneous tissue is below the skin surface initial temperature. Figure 20 also shows that increased blood perfusion gives a temperature mean value near the temperature of the skin surface at time $t = 0$ s.

4 Conclusion

Using Fourier series method, we built the series solution for temperature distribution in biological tissue, simultaneously subjected to oscillatory surface and spatial heating, when blood perfusion is temperature-independent. Based on truncated analytical series solution, we studied temperature distribution in muscle, tumor and fat tissue by varying different blood parameters and heat source parameters. The numerical

simulations based on the second-order central difference scheme in space and the Crank–Nicholson type of scheme in time are used to investigate the temperature distribution in muscle, tumor and fat tissue, as well as is dermis and subcutaneous when blood perfusion is temperature-dependent. The obtained analytical series solution and numerical have more capability to deal with many practical bioheat transfer problems than quite a few existing analytical solutions. In fact, the surface and the spatial heating used in this work include most of the possible external heating style (simultaneously spatial and surface heating, oscillatory surface heating, oscillatory spatial heating, constant surface heating, ...). The analytical and the numerical solution presented in this work are useful (for example, one can easily describe the tissue temperature response in a one-dimensional domain using the analytical series solution) and can be used to predicate the evolution of the detailed temperature within the tissues during thermal therapy.

References

[1] M. Blevins and G.W. Stewart. Calculating the eigenvectors of diagonally dominant matrices. *J. Assc. Comp. Mach.* **21** No 2 (1974), 261–271.

[2] W. Dai, A. Bejan, X. Tang, L. Zhang, and R. Nassar. Optimal temperature distribution in a three dimensional triple-layered skin structure with embedded vasculature. *J. Appl. Phys.* **99** (2006), 104702-1–104702-9.

[3] Z.-S. Deng and J. Liu. Analytical study on bioheat transfer problems with spatial or transient heating on skin surface or Inside biological bodies. *J. Biomech. Eng.* **124** (2002), 638–649.

[4] T.E. Dudar and R.K. Jain. Differential response of normal and tumor microcirculation to hyperthermia. *Cancer Res.* **44** (1984), 605–612.

[5] T.M.N. El-dabe, M.A.A. Mohamed, and A.F. El-Sayed. Effects of microwave heating on the thermal states of biological tissues. *African Journal of Biotechnology* **2** No 11 (2003), 453-459.

[6] K.S Frahm, O.K. Andersen, L. Arendt-Nielsen, and C.D. Mørch. Spatial temperature distribution in human hairy and glabrous skin after infrared CO2 laser radiation. *BioMedical Engineering OnLine* **9** (2010), 1-9.

[7] T.R Gowrishankar, D.A. Stewart, G.T. Martin, and J.C. Weaver. Transport lattice models of heat transport in skin with spatially heterogeneous, temperature-dependent perfusion. *BioMedical Engineering OnLine* **3** (2004), 42.

[8] K.R. Holmes. Biological structures and heat transfer. In: *The future of biothermal engineering, Allerton Workshop, University of Illinois*, (1997), 14–37.

[9] M. Jain and M. Shakya. Study of temperature variation in human peripheral region during wound healing process due to plastic surgery. *Applied Mathematical Sciences*, **3** No.54 (2009), 2651–2662.

[10] E. Kengne, A. Lakhssassi, and R. Vaillancourt. Temperature Distributions for Regional Hypothermia Based on Nonlinear Bioheat Equation of Pennes Type: Dermis and Subcutaneous Tissues. Applied Mathematics 3 (2012), 217-224.

[11] A. Lakhssassi, E. Kengne, and H. Semmaoui. Modifed Pennes' equation modelling bio-heat transfer in living tissues: analytical and numerical analysis. *Natural Science* **2** No. 12 (2010), 1375–1385.

[12] A. Lakhssassi, E. Kengne, and H. Semmaoui. Investigation of nonlinear temperature distribution in biological tissues by using bioheat transfer equation of Pennes' type. *Natural Science*, **2** No. 3 (2010), 131–138.

[13] J. Lang, B. Erdmann, M. Seebass. Impact of nonlinear heat transfer on temperature control in regional hyperthermia. *IEEE Trans. on Biomedical Engineering*, (1999), 1129–138.

[14] J. Liu and L.X. Xu. Estimation of blood perfusion using phase shift in temperature response to sinusoidal heating at the skin surface. *IEEE Trans. Biomed. Eng.* **46** (1999), 1037–1043.

[15] D. Park, N.H. Seung, J. Kim, H. Jeong, and S. Lee. Infrared thermography in the diagnosis of unilateral carpal tunnel syndrome. *Muscle Nerve*, **36** (2007), 575–576.

[16] H.H. Pennes. Analysis of tissue and arterial blood temperature in the resting forearm. *J. Appl. Physiol.* **1** (1948), 93–122.

[17] V.P. Saxena and K.R. Pardasani. Effect of dermal tumours on temperature distribution in skin with variable blood flow. *Bull. Math. Biol.* **53** No. 4 (1991), 525–536.

[18] T.-C. Shih, P. Yuan, W.-L. Lin, H.-S. Kou. Analytical analysis of the Pennes bioheat transfer equation with sinusoidal heat flux condition on skin surface. *Medical Engineering & Physics* **29** (2007), 946–953.

[19] V. Shusterman, K.P. Anderson, and O. Barnea. Spontaneous skin temperature oscillations in normal human subjects. *Am. J. Physiol. Regul. Integr. Comp. Physiol.*, **273** (1997), R1173–R1181.

[20] C.W. Song. Effect of local hyperthermia on blood flow and microenvironment: a review. *Cancer Res* **44** (1984), 4721S–4730S.

[21] C.W. Song, A. Lokshina, J.G. Rhee, M. Patten, and S.H. Levitt. Implication of blood flow in hyperthermic treatment of tumors. *IEEE Trans. Biomed. Eng.* **31** (1984), 9–16.

[22] L. Weibel, M.C. Sampaio, M.T. Visentin, K.J. Howell, P. Woo, and J.I. Harper. Evaluation of methotrexate and corticosteroids for the treatment of localized scleroderma (morphoea) in children. *Br. J. Dermatol.*, **155** (2006), 1013–1020.

[23] S. Weinbaum, L.M. Jiji, and D.E. Lemons. Theory and experiment for the effect of vascular microstructure on surface tissue heat transfer-part I: Anatomical foundation and model conceptualization. *ASME J. Biomech. Eng.* **106** (1984), 321–330.

[24] F.M.M. Ya'Ish, J.P. Cooper, and M.A.C. Craigen. Thermometric diagnosis of peripheral nerve injuries - Assessment of the diagnostic accuracy of a new practical technique. *J. Bone Joint Surg.*, **89B** (2007), 933–939.

Received: March, 2012